frontiers | Frontiers in Photonics

TYPE Review
PUBLISHED 13 February 2024
DOI 10.3389/fphot.2024.1331030

OPEN ACCESS

EDITED BY
Marisa Di Sabatino,
Norwegian University of Science and Technology, Norway

REVIEWED BY
Tsung Sheng Kao,
National Yang Ming Chiao Tung University, Taiwan
Bruno Ceccaroli,
Independent Researcher, Oslo, Norway

*CORRESPONDENCE
Nerea Dasilva Villanueva,
cn.dasilva@upm.es

RECEIVED 31 October 2023
ACCEPTED 17 January 2024
PUBLISHED 13 February 2024

CITATION
Míguez Novoa JM, Hoffmann V, Forniés E, Mendez L, Tojeiro M, Ruiz F, Funes M, del Cañizo C, Fuertes Marrón D, Dasilva Villanueva N, Caballero LJ, Arıkan B, Turan R, Canar HH and Sánchez Plaza G (2024), Production of upgraded metallurgical-grade silicon for a low-cost, high-efficiency, and reliable PV technology.
Front. Photonics 5:1331030.
doi: 10.3389/fphot.2024.1331030

Production of upgraded metallurgical-grade silicon for a low-cost, high-efficiency, and reliable PV technology

José Manuel Míguez Novoa[1], Volker Hoffmann[1], Eduardo Forniés[2], Laura Mendez[2], Marta Tojeiro[2], Fernando Ruiz[2], Manuel Funes[2], Carlos del Cañizo[3], David Fuertes Marrón[3], Nerea Dasilva Villanueva[3]*, Luis Jaime Caballero[3], Bülent Arıkan[4], Raşit Turan[4,5], Hasan Hüseyin Canar[4,6] and Guillermo Sánchez Plaza[7]

[1]FerroGlobe, Arteixo, Spain, [2]Aurinka PV Group, Rivas-Vaciamadrid, Spain, [3]Instituto de Energía Solar, ETSI Telecomunicación, Universidad Politécnica de Madrid, Madrid, Spain, [4]ODTÜ-GÜNAM (Center for Solar Energy Research and Applications), Ankara, Turkiye, [5]Department of Physics, Middle East Technical University, Ankara, Turkiye, [6]Micro and Nanotechnology, Middle East Technical University, Ankara, Turkiye, [7]Nanophotonics Technology Center–Universidad Politécnica de Valencia, Valencia, Spain

Upgraded metallurgical-grade silicon (UMG-Si) has the potential to reduce the cost of photovoltaic (PV) technology and improve its environmental profile. In this contribution, we summarize the extensive work made in the research and development of UMG technology for PV, which has led to the demonstration of UMG-Si as a competitive alternative to polysilicon for the production of high-efficiency multicrystalline solar cells and modules. The tailoring of the processing steps along the complete Ferrosolar's UMG-Si manufacturing value chain is addressed, commencing with the purification stage that results in a moderately compensated material due to the presence of phosphorous and boron. Gallium is added as a dopant at the crystallization stage to obtain a uniform resistivity profile of ~1 Ω cm along the ingot height. Defect engineering techniques based on phosphorus diffusion gettering are optimized to improve the bulk electronic quality of UMG-Si wafers. Black silicon texturing, compatible with subsequent gettering and surface passivation, is successfully implemented. Industrial-type aluminum back surface field (Al-BSF) and passivated emitter and rear cell (PERC) solar cells are fabricated, achieving cell efficiencies in the range of those obtained with conventional polysilicon substrates. TOPCon solar cell processing key steps are also tested to further evaluate the potential of the material in advanced device architectures beyond the PERC. Degradation mechanisms related to light exposure and operation temperature are shown to be insignificant in UMG PERC solar cells when a regeneration step is implemented, and PV modules with several years of outdoor operation demonstrated similar performance to reference ones based on poly-Si. Life cycle analysis (LCA) is carried out to evaluate the environmental impact of

10.3389/fphot.2024.1331030

UMG-based PV technology when compared to poly-Si-based technology, considering different scenarios for both the manufacturing sites and the PV installations.

KEYWORDS

photovoltaic solar energy, silicon feedstock, metallurgical route, solar-grade silicon, solar cell manufacturing, module degradation, life cycle assessment

1 Introduction

In 2000, the Spanish company Ferroatlántica, one of the key manufacturers of metallurgical silicon worldwide, started a research program for the production of solar-grade silicon. Anticipating the silicon shortage already on the horizon due to the growth of the photovoltaic (PV) market (Aulich and Schulze, 2002), Ferroatlántica (now Ferroglobe after the merger with the American company Globe Specialty Metals) aimed at upgrading its silicon to meet the requirements of the PV industry by applying "metallurgical methods," an interesting approach with the potential to reduce energy consumption and associated costs, as compared to the incumbent Siemens technology. Ferroatlántica designed its own route based on the knowledge accumulated by the sector in the 1970s–1980s under several programs funded in the USA, Japan, and Europe after the oil crisis (Dietl, 1987). A small pioneer ingot was grown by the Institut für Kristallzüchtung (IKZ) with the first batch of upgraded silicon produced by Ferroatlántica. It was a compensated p-type material with a resistivity of 0.015 Ω cm due to the large amount of B contained in the feedstock, and it also incorporated a high amount of other impurities. Laboratory-type P/Al-BSF solar cells were fabricated at the Instituto de Energía Solar in Universidad Politécnica de Madrid to complete a whole manufacturing cycle, from metallurgical Si to solar cell fabrication. The recorded device efficiency was 10.7%, and the comparison of the quantum efficiency with that of a multicrystalline solar cell made from conventional electronic-grade polysilicon (Figure 1) clearly showed the limit imposed by the substrate quality (Del Cañizo et al., 2005).

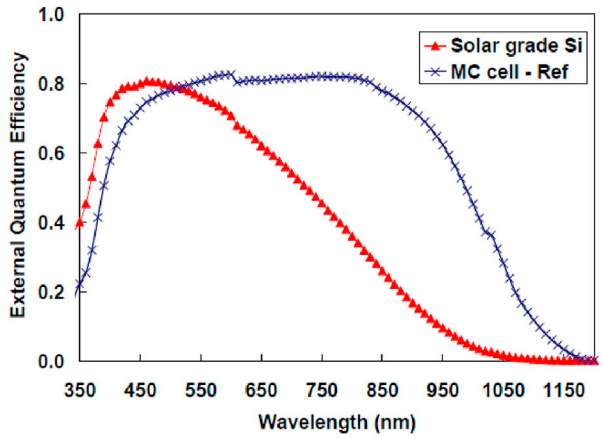

FIGURE 1
External quantum efficiency of a P/Al-BSF solar cell made with wafers from the first ingot grown with Ferroatlántica's solar-grade silicon (red) in comparison with a reference made on conventional multicrystalline material (blue). The figure was reproduced from the work of Del Cañizo et al. (2005), with permission from the EUPVSEC.

In 2017, Ferroglobe and Aurinka PV Group formed a joint venture called Ferrosolar to take advantage of the acquired knowledge of metallurgical processes from Ferroglobe and the techno-economic experience from Aurinka in the solar industry. After a sustained R&D effort, industrial-type multicrystalline PERC solar cells fabricated on the solar silicon purified by Ferrosolar have already surpassed the 20% efficiency target, and PV modules with these cells have been in operation for several years, demonstrating similar energy generation performance to that of neighboring reference modules made from conventional polysilicon (Forniés et al., 2021).

The upgraded metallurgical technology was then ready for commercialization by the end of the last decade, and Ferrosolar planned to start industrial production of its solar-grade silicon in Puertollano, Spain. Unfortunately, the initiative was stopped due to unfavorable market conditions. Despite this fact, the technology has successfully demonstrated its potential to reduce capital expenditure (CAPEX), manufacturing costs, and energy consumption for the fabrication of PV devices, as compared to those based on conventional polysilicon, and further developments are foreseen to keep up with the continuous progress that crystalline silicon technology is making.

This paper updates the achievements of the solar-grade silicon technology developed by the Ferrosolar project in Spain, reviewing its most relevant characteristics and assessing its environmental performance.

2 The upgraded metallurgical silicon value chain, from feedstock to PV modules

The silicon feedstock purified by a sequence of metallurgical steps, thereby avoiding the chemical transformation into intermediate species (such as trichlorosilane in the dominant technology), has been referred to as upgraded metallurgical silicon (UMG or UMG-Si) (Ceccaroli et al., 2017). A number of initiatives advanced in the development of UMG-Si in the 2000s (Yuge et al., 2001; Øvrelid et al., 2006; Hoffmann et al., 2008; Modanese et al., 2011; Cocco et al., 2013). Some of them reached the market but could not survive long due to the reaction of the polysilicon industry that quickly expanded capacity and introduced processing optimizations, thus lowering manufacturing costs as compared to those achieved when serving just the microelectronic industry. Ferrosolar in Spain was among the main players following the UMG route. In the next sections, the

10.3389/fphot.2024.1331030

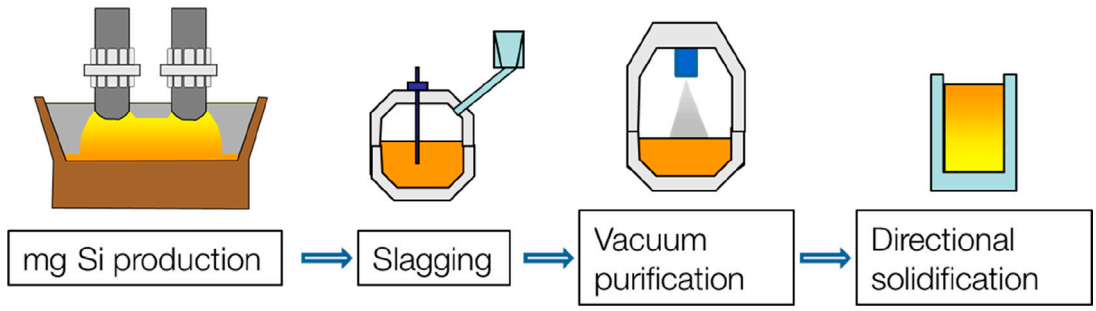

FIGURE 2
Sketch of the main steps in the upgrade of metallurgical silicon. The figure was reproduced from the work of Del Cañizo et al. (2023) with permission from the EUPVSEC.

stage of technological development of its UMG-Si is reported, along with an analysis of its performance over the entire value chain, from the feedstock to the module.

2.1 Feedstock production

The main steps involved in the silicon purification process resulting in UMG-Si are sketched in Figure 2 and are described in detail in previous works (Hoffmann et al., 2015; Forniés et al., 2018). The process begins with the selection and cleaning of raw materials that will be reduced in the arc furnace to produce metallurgical silicon. The process concatenates several steps that include slagging to reduce the high initial boron content, vacuum evaporation to reduce the similarly high initial phosphorus content, and directional solidification to crystallize UMG-Si ingots and simultaneously remove metallic impurities.

The resulting UMG-Si product is characterized by a boron concentration below 0.2 ppmw, a phosphorus concentration in the range of 0.1–0.3 ppmw, and a total metal impurity concentration below 0.5 ppmw, which has been confirmed as a reasonable starting point for the production of competitive solar silicon feedstock.

2.2 Crystallization and wafering: characterization before and after defect engineering

High-performance multicrystalline ingots can be grown using this silicon feedstock. As both boron and phosphorus are present in UMG-Si, the different rates of incorporation from the liquid to the solid, due to their different segregation coefficients, would result in large variations of net doping concentration and electric resistivity along the ingot and even a change of doping character, from p-type to n-type material, at the top of the ingot. This undesired feature should, thus, be corrected by adding controlled quantities of the additional dopants Ga (from 5 to 10 ppmw) and P (0.12 ppmw) to the melt. The impact of the dopant addition is exemplified in Figure 3A, where the expected resistivity profile of two ingots, one without the addition of gallium and the other with it, is modeled. Figure 3B shows the experimentally observed resistivity profiles of two different UMG-Si bricks grown at Pillar in Ukraine following this dopant-addition strategy.

Carrier lifetime maps of complete ingots measured with the Semilab WT-2000P tool are shown in Figure 4A. Discarding the top and bottom parts of each ingot due to the high concentration of impurities, the measured average effective lifetimes are around 6 µs.

Ingots should then be further cut into bricks and sliced into wafers. All the experimental tests below are performed on 156.75 × 156.75 mm^2 and 180-µm-thick wafers.

Injection-dependent carrier lifetimes at the wafer level are measured by photoconductance decay (PCD) using the Sinton Instruments WCT-120 tool after passivating the surfaces by immersion in a 0.1 M iodine–ethanol (I–E) solution. Very low lifetimes, in the 1 µs range, are typically obtained from bare wafers, as shown in Figure 4B, a clear indication that the material quality is limited by the presence of a large concentration of contaminant impurities. At low injection levels, trapping effects commonly observed in multicrystalline materials are clearly seen. The impact of carrier trapping in UMG-Si has been analyzed in detail elsewhere (Catalán-Gómez et al., 2021; Dasilva-Villanueva et al., 2022).

To effectively remove impurities from the bulk of the UMG-Si wafers, particularly those of metallic character, a phosphorous diffusion gettering (PDG) step is introduced prior to cell processing. For this purpose, a test was carried out for selecting wafers randomly from different bricks cut from three different ingots to account for positional effects and batch variability. They were cut into 52 × 52 mm^2 samples and first characterized with the Sinton tool and then chemically treated with CP4 (HNO_3/HF) etching, RCA1 ($NH_4OH/H_2O_2/H_2O$) surface cleaning, and a treatment in 2% HF to ensure native oxide removal before the thermal process.

P-diffusion was then performed in a tubular furnace under different processing times (30, 60, and 90 min) and temperatures (780°C, 800°C, 820°C, and 850°C). The diffusion was followed by a 10-min drive-in at the same temperatures. The P-source was liquid $POCl_3$ kept at 26°C, assuring super-saturation conditions during the diffusion step. After PDG, the emitter formed atop the surface was removed by chemical etching, and PCD measurements were conducted again.

The impact of sequential PDG processes carried out under different conditions (durations and temperatures) on the bulk

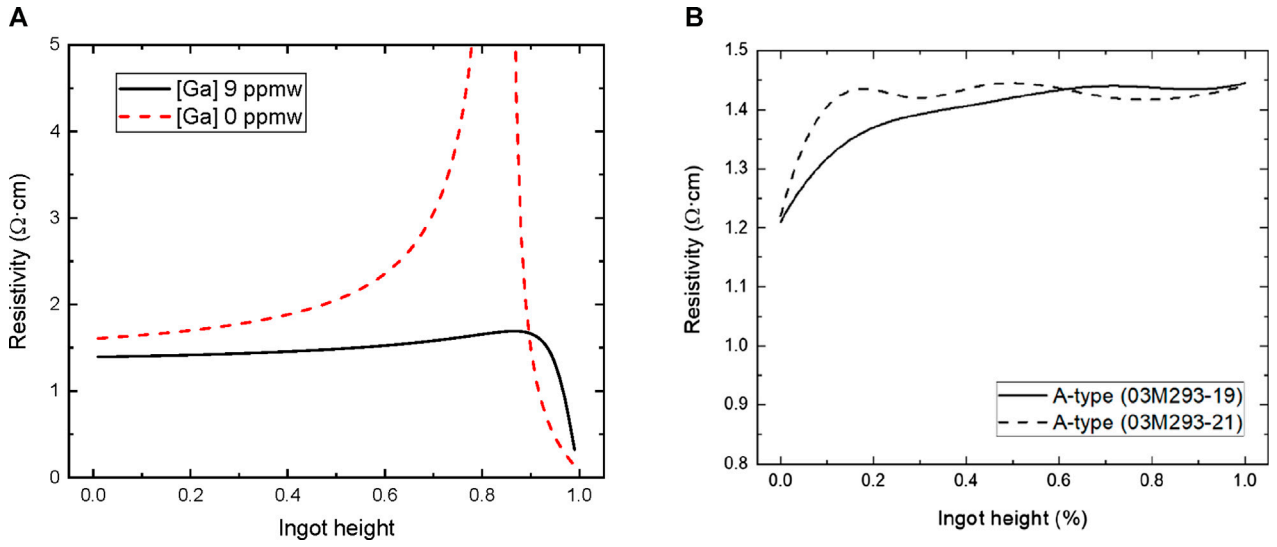

FIGURE 3
(A) Calculated resistivity profiles applying Klaassen's mobility model to two ingots with B and P concentrations of 0.17 and 0.42 ppmw, respectively, with no addition of Ga (dashed line) and adding 9 ppmw of Ga (straight line). **(B)** Experimental resistivity profiles measured in two UMG-Si bricks grown at pillar with those concentrations.

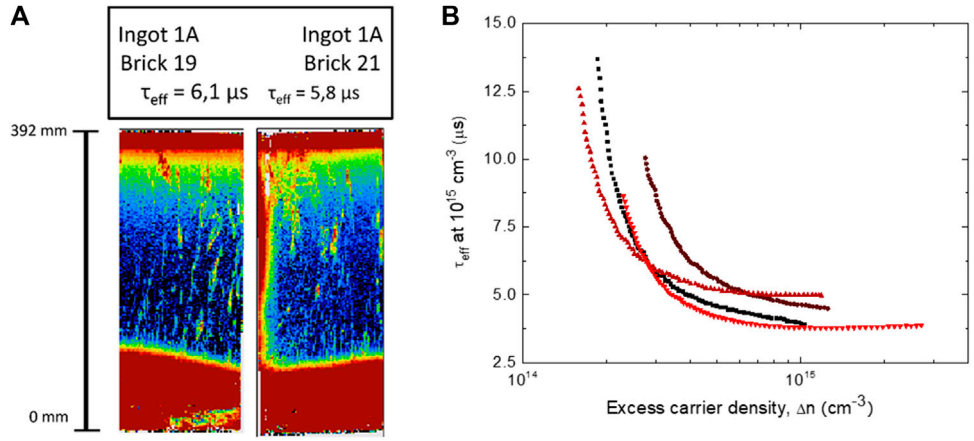

FIGURE 4
(A) Lifetime mappings of two UMG-Si ingots grown at pillar as HPMC. The figure was reproduced from the work of Forniés et al. (2021) with permission from Elsevier. **(B)** Injection-dependent effective carrier lifetime of IE-passivated UMG-Si wafers.

carrier lifetime of UMG-Si at a carrier injection level of $\Delta n = 10^{15}$ cm^{-3}, as can be seen in Figure 5. The best results for the first gettering process are systematically obtained at a "low" temperature (780°C), resulting in lifetimes upgraded to an average level of 300 µs. Further improvements can be observed after a second PDG process, reaching an outstanding maximum lifetime of 722 µs. It is also interesting to note that this second P-diffusion provides an efficient gettering effect under a relatively wide range of temperatures, in particular and most conveniently, those compatible with P-diffusion processes for emitter provision and subsequent cell processing.

2.3 Solar cell development and results

The characterization program conducted on UMG-Si wafers led to conclude that they could feed a solar cell manufacturing process compatible with industrial upscaling. Three cell architectures have been tested for this purpose: Al-BSF, PERC, and TOPCore. In the first two cases, large-area (156.75 × 156.75 mm^2) solar cells were fabricated in industrially compatible production lines. In the third case, TOPCon key processing steps have been tested on the material to evaluate its potential beyond PERC.

10.3389/fphot.2024.1331030

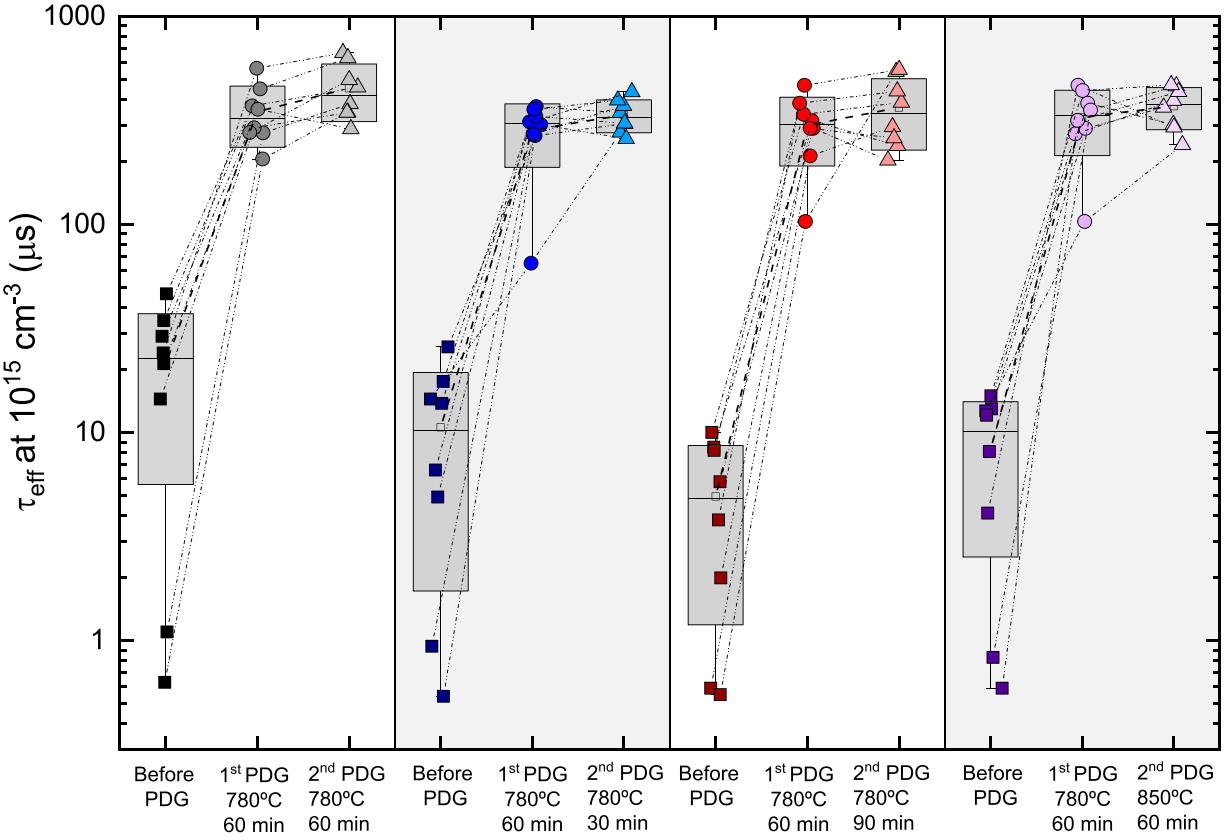

FIGURE 5
Effective lifetime variation before PDG, after one PDG process, and after two PDG processes for different conditions of iodine–ethanol-passivated UMG-Si samples. In the box-type plot, whiskers represent max–min variation, the height of the box represents the standard deviation, the non-filled square corresponds to the mean value, and the middle line represents the median value. Connection dashed lines are included to identify the change of individual samples. The figure was reproduced from the work of Del Cañizo et al. (2023) with permission from the EUPVSEC.

2.3.1 Al-BSF solar cells

The first stage in the manufacturing of multicrystalline Al-BSF solar cells by a tier-1 producer consists of saw damage removal and conventional acidic texturing. The P-emitter diffusion is performed in a low-pressure diffusion furnace, and a back-side chemical etching is performed to remove the diffused phosphorus from the back side, followed by an additional chemical etching for edge isolation. Thermal annealing follows to form a thin silicon dioxide to increase the resilience against potential-induced degradation (Luo et al., 2017) of complete devices in operation, and subsequently, the silicon nitride antireflective coating is deposited by plasma-enhanced chemical vapor deposition (PECVD). Front and rear contacts, as well as the aluminum coating responsible for the back surface field (BSF) formation, are printed in a double printing process, and a co-firing furnace is used to induce the drive-through of the contacts (Ballif et al., 2002).

The performance of UMG-Si cells is compared in Table 1 with that of cells based on polysilicon wafers processed in the same batch. It should be noted that no tuning of the manufacturing parameters was implemented so as to adapt the cell fabrication to the peculiarities of the incoming UMG-Si wafers; in particular, no additional PDG step was implemented, just the conventional diffusion to diffuse the *p* emitter.

2.3.2 PERC solar cells

An industrially compatible process was designed for large-area PERC solar cells (Figure 6), optimizing the different steps for UMG-Si on the pilot scale at ODTÜ-GÜNAM.

After saw damage removal in an alkaline bath, a PDG step is implemented, as suggested by the optimization carried out in section 2.2, after which the wafers are symmetrically etched to remove the phosphosilicate glass (PSG) and the diffused emitter.

Metal (silver)-assisted chemical etching (MACE) is implemented to texture the wafers. The appearance of the UMG-Si wafer surface before and after MACE nanotexturing is shown in Figure 7. As can be observed, the overall surface reflectance has decreased significantly after the treatment and the surface looks almost black. A SEM image of the MACE nanotextured surface is shown in Figure 7C.

The highly textured surface must then be prepared for the subsequent creation of a high-quality, effectively passivated emitter by means of a chemical acidic etching step. This step represents a delicate tradeoff between a high aspect ratio and good surface passivation and proceeds with a gentle smoothing of the nm-size surface features (thus leading to slightly increased surface reflectance) that permits an enhanced passivation efficacy. The treatment also eliminates the texturing from the cell's rear side.

10.3389/fphot.2024.1331030

TABLE 1 Average values of solar cell production. Comparison between polysilicon and UMG-Si for Al-BSF technology. The dashes in the cells stand for data not provided by the producer. The column red. ($\%_{ref}$) refers to the relative reduction in efficiency between UMG and poly (Forniés et al., 2019).

Solar cell results		P_{MPP} [W]	V_{oc} [V]	I_{sc} (A)	FF (%)	Eta (%)	Red. ($\%_{ref}$) (%)	Counts
A1-BSF	Poly	4.543	0.633	8.98	79.63	18.490	0.47	-
	UMG	4.522	0.632	9.02	79.27	18.404		99,692

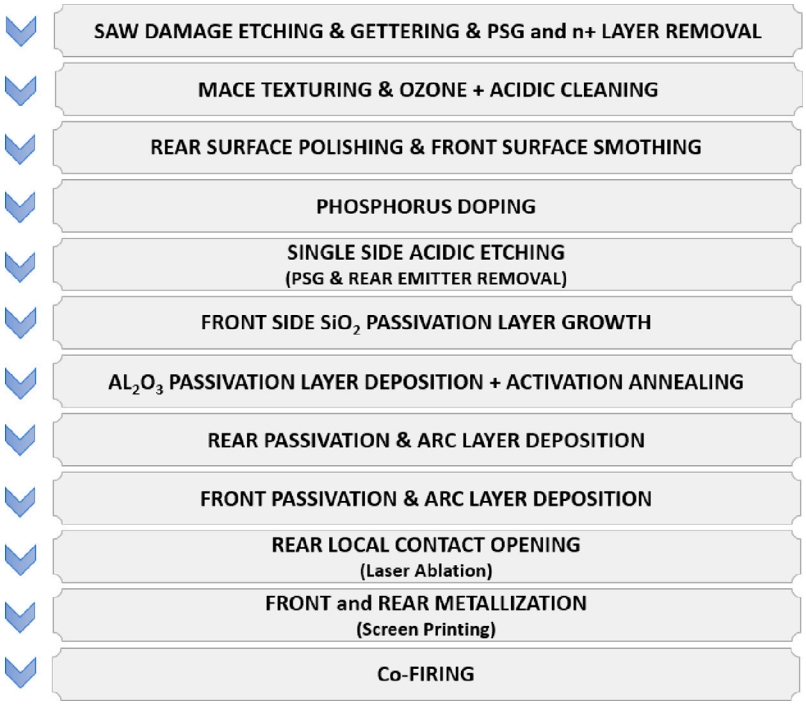

FIGURE 6
UMG-Si PERC solar cell process flow in an industrially compatible pilot line.

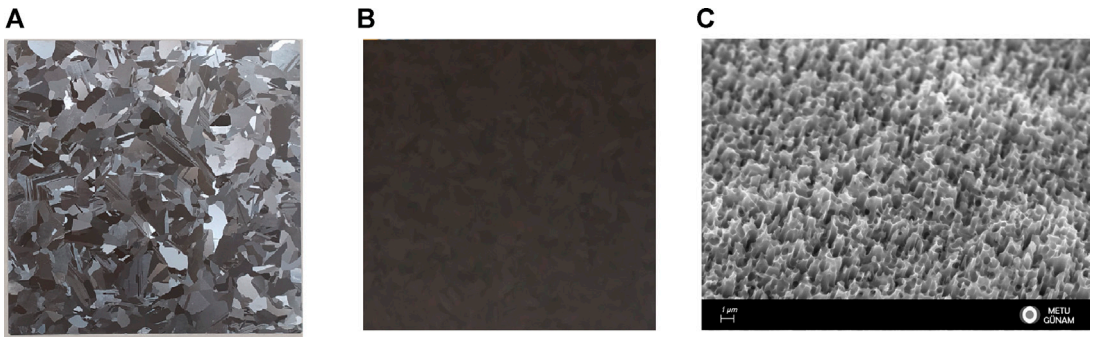

FIGURE 7
(A) Saw damage etched mc-UMG wafer. **(B)** mc-UMG wafer after MACE. **(C)** SEM image of the MACE nanotextured surface.

After the smoothing process, grains with different orientations show relatively different reflectance. A comparison between measurements performed before and after smoothing on different grains is shown in Figure 8. The average reflectance value was determined in the range of 11.5–12%, similar to reflectance values obtained from pyramidal alkaline texturing. As can be observed, the optical response at short wavelengths following the MACE approach is improved compared to the standard pyramidal approach.

A phosphorus emitter was subsequently diffused from a $POCl_3$ source in a tubular furnace, testing some recipes that resulted in

10.3389/fphot.2024.1331030

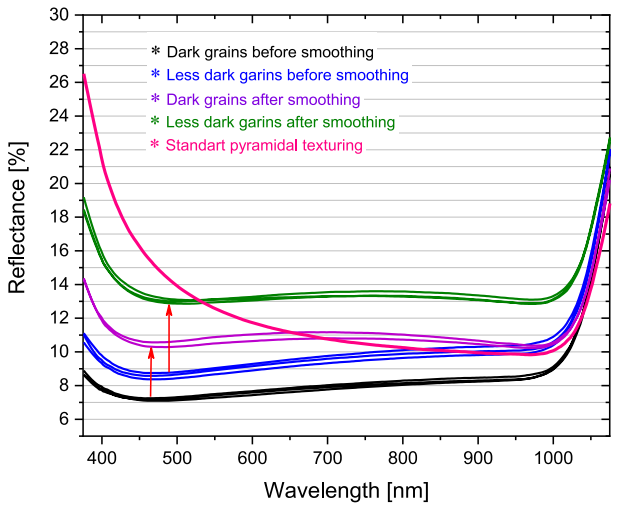

FIGURE 8
Reflectance measurements on different grains of MACE-textured mc-UMG wafers before and after the chemical smoothing step. The reflectivity of a sample with standard pyramidal texturing is shown as a reference.

sheet resistances in the range of 80–100 Ω/□. A single-side etch was then performed to remove the phosphosilicate glass (PSG) and the rear diffused region.

Different passivation layer stacks were tested both on MACE-textured n+ doped front surfaces and polished p-type rear surfaces to finally reach the structures sketched in Figure 9. As for the front surface, a stack formed by a hydrogenated amorphous silicon oxynitride (a-SiO_xN_y:H) layer and hydrogenated amorphous silicon nitride (a-SiN_x:H) gave the best results, provided a thin silicon oxide layer was previously grown at low temperature (600°C) on the emitter. A 2-stack version (Figure 9A) and a 4-stack version (Figure 9B) tuning indexes of refractions and layer thicknesses are implemented. As for the rear side, the atomic layer deposition (ALD) of thin alumina was chosen as the first passivating layer, after which a 20 nm hydrogenated amorphous silicon oxynitride (a-SiOxNy:H) layer plus a 100 nm hydrogenated amorphous silicon nitride (a-SiNx:H) capping layer were deposited by plasma-enhanced chemical vapor deposition (PECVD).

Rear local contact opening was performed via laser ablation, covering a 3.19% fraction of the rear surface, which was determined as optimum from both simulation and experimental studies.

Regarding the screen-printing metallization and firing, a 5-busbar, 129-finger silver metallization pattern was applied on the front surface and a full aluminum metallization pattern was applied at the rear. Problems arose in the form of discontinuities and narrowing of the metal fingers (see Figure 10) due to the use of pastes developed and optimized for pyramidal textured surfaces and would be solved with new-generation pastes and masks to be developed for nanotextured surfaces.

Solar cell parameters measured after completion under standard test conditions are shown in Figure 11. Due to PDG and the rear and front passivation layer stacks, V_{oc} values as high as 659 mV have been reached, in line with values routinely achieved with conventional polysilicon-based multicrystalline PERC cells in the same production line. Maximum J_{sc} and FF values read 38.2 mA/cm^2 and 80.3%, respectively, slightly lower than those typically obtained with commercial industrial PERC cells and attributed to the use of pastes that are not optimized for nanotextured surfaces, as already explained, also responsible of the relatively wide distribution of values observed. Notwithstanding, a top cell efficiency of 20.1% has been achieved, a mark that could be further improved with the use of appropriate metal pastes and the implementation of additional advanced features, such as selective emitters or floating busbars.

Additionally, the impact of light-induced degradation (LID) and light and elevated temperature-induced degradation (LeTID) mechanisms is evaluated on these cells. I-V and SunsV_{oc} measurements of the fabricated cells were performed after firing, and the samples were kept under light (sunlight) at room temperature for controlled degradation. Regeneration was then performed on the degraded cells under optimized conditions (2 hours under sunlight with an intensity of 1 sun at 140°C). Regarding LID, in controlled tests, a degradation of up to 5 mV in V_{oc} from the initial value was observed, but applying a light and heat source assisted the regeneration process, the V_{oc} degradation was successfully reverted, and the initial values were restored. As for the LeTID, for the time being, no long-term tests have been completed yet, but short-term tests have shown no measurable effect.

Similar results are obtained by a tier-1 solar cell producer in its industrial pilot line, with the processing of a large number of UMG-Si multi wafers (more than 45.000) following no specific tuning of production parameters as to adapt them to UMG material. No pre-gettering step was included in this case. After saw damage removal, a black silicon nanotexture etching is performed by reactive ion etching (RIE). Phosphorus diffusion, back-side emitter removal, edge isolation, and annealing followed, similar to the previous case. The characteristic back surface passivation of PERC cells was implemented, consisting of a thin Al_2O_3 film plus a SiN_x capping layer, both deposited by PECVD. Backside openings through the passivation stack were made by a nanosecond pulsed laser, and the screen-printing metallization followed. To minimize the light and elevated temperature degradation (LeTID), a post-treatment processing of the cells is performed.

The average parameters of the manufactured solar cells are shown in Table 2, comparing those obtained with UMG-Si wafers and those with polysilicon wafers processed in the same test. The record efficiency (not shown in the table) is 20.8 %.

Some of these PERC solar cells are tested for LeTID following the IEC TS 63342 norm (IEC, 2022) to assess whether the preventive treatment applied to avoid it is indeed effective. As depicted in Figure 12, V_{oc} readings reflect an initial decrease right after current injection and a gradual recovery of the cell voltage afterward. The cell was preconditioned to avoid the influence of B-O complexes during the test and then measured to determine its output power. Once the treatment was stopped, the power was measured again, confirming a power reduction below 3% with respect to the starting values. This result leads to conclude that the preventive treatment was successful in making the mc-UMG-based PERC cell LeTID-insensitive.

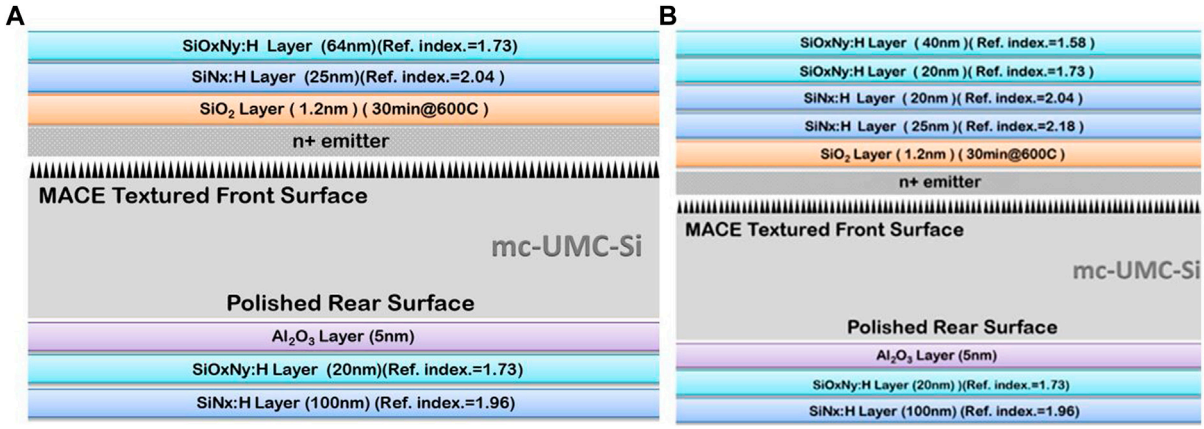

FIGURE 9
Proposed passivation structures for the front and rear surfaces of UMG PERC cells. **(A)** 2-stack on a SiO_2 layer. **(B)** 4-stack on a SiO_2 layer.

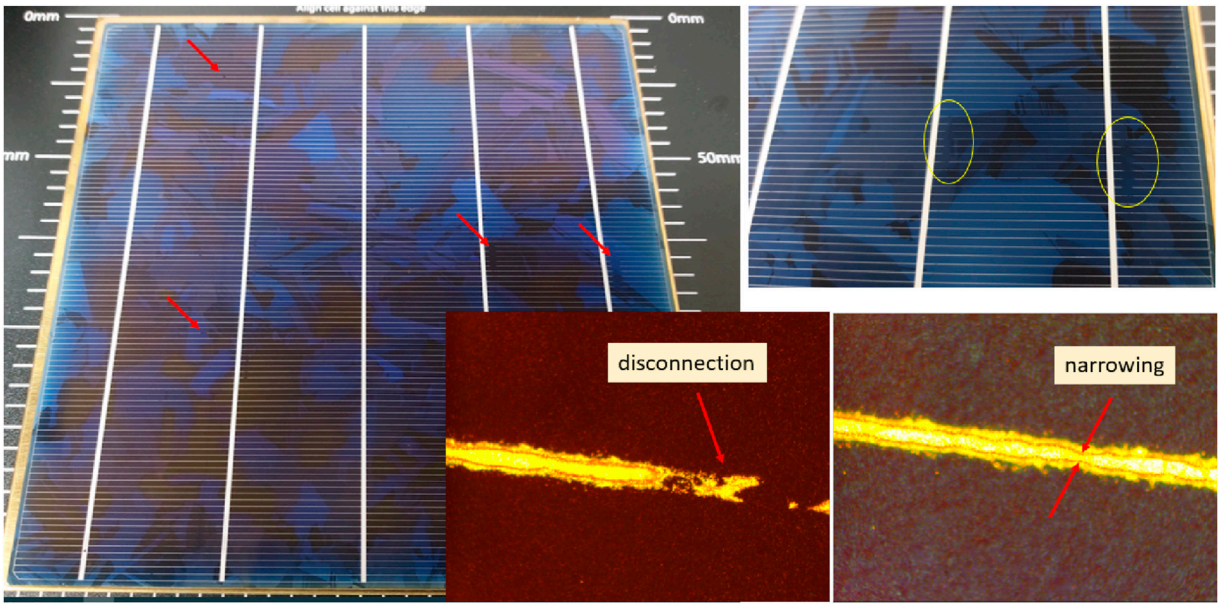

FIGURE 10
Major metal printing problems identified on MACE-textured PERC cells.

2.3.3 TOPCoRE solar cells

To further assess the potential of UMG to keep up and follow the rapid evolution of silicon technology, additional experiments were performed at Fraunhofer ISE to implement TOPCon rear emitter structure (TOPCoRE) (Richter et al., 2021) on the UMG-Si substrates.

As a first step, bulk lifetimes after PDG- and TOPCon-compatible annealing were measured by calibrated photoluminescence (PL), confirming carrier lifetime values in the range of hundreds of microseconds from most of the area of the processed wafers, even locally surpassing the millisecond in some regions.

The samples were satisfactorily plasma-textured, achieving a reflectance (without ARC) below 5.9% in the range of 300 to 1,000 nm. Excellent surface passivation could be reached on these textured surfaces by means of Al_2O_3/SiN_x layer stacks, yielding implied V_{oc} >700 mV in good areas of the processed wafers.

Based on injection-dependent PL results, an efficiency-limiting bulk recombination analysis (ELBA) is conducted in order to infer local PV efficiency distributions over the probed sample area (Michl et al., 2012). As shown in Figure 13, a global efficiency above 22% is within reach with these multicrystalline UMG-Si substrates.

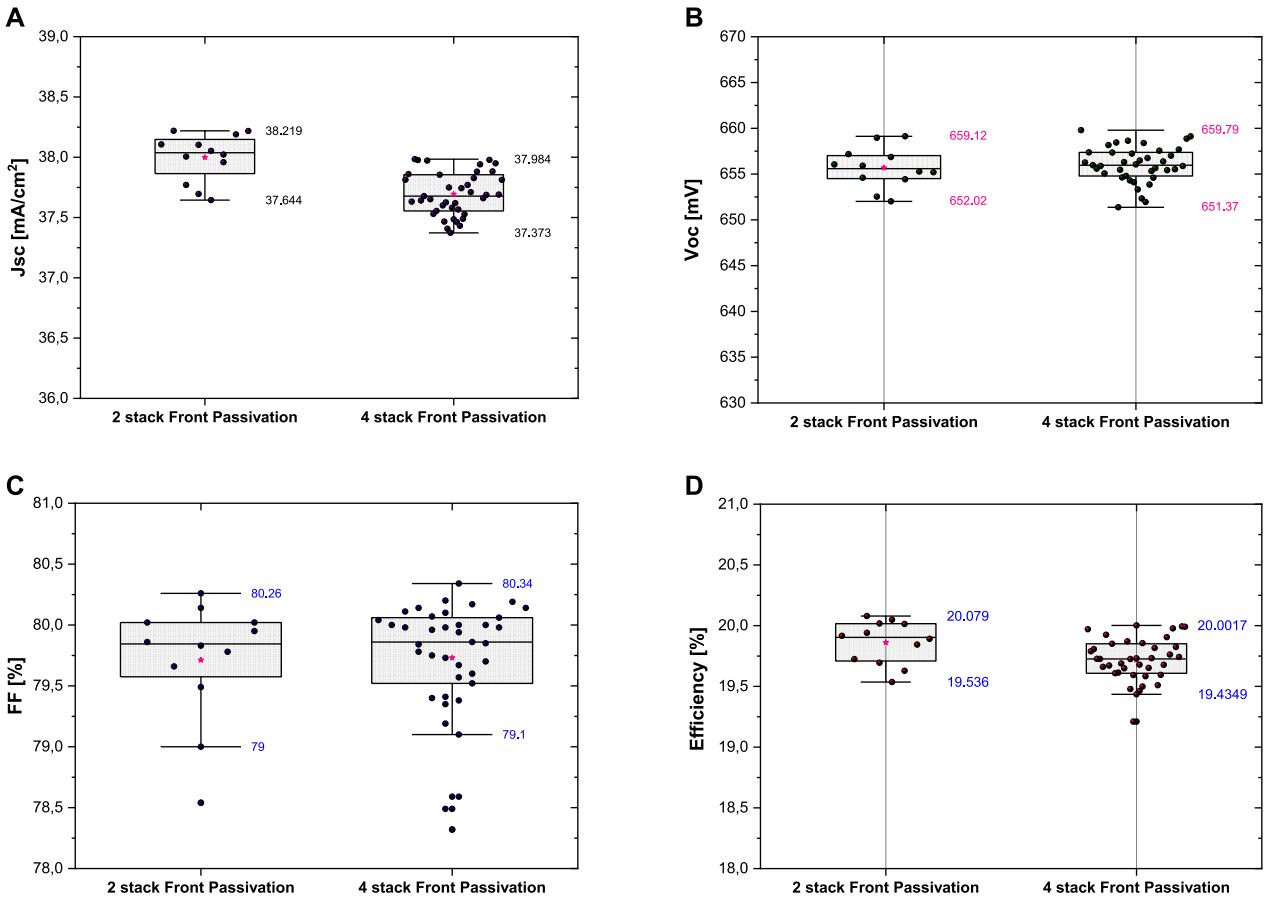

FIGURE 11
UMG-Si PERC solar cell parameters processed at the ODTÜ-GÜNAM pilot line, measured under standard test conditions. **(A)** Short-circuit current density (J_{sc}). **(B)** Open-circuit voltage (V_{oc}). **(C)** Fill factor (FF). **(D)** Efficiency. The figure was reproduced from the work of Del Cañizo et al. (2023) with permission from the EUPVSEC.

TABLE 2 Average values of solar cell production. Comparison between polysilicon and UMG-Si for PERC technology. The column red. ($\%_{ref}$) refers to the relative reduction in efficiency between UMG and poly (Forniés et al., 2019).

Solar cell results		P_{MPP} [W]	V_{oc} [V]	I_{sc} [A]	FF (%)	Eta (%)	Red. ($\%_{ref}$) (%)	Counts
B-Si (RIE) + PERC	Poly	5.014	0.7	9.62	80.02	20.410	1.37	55,396
	UMG	4.945	0.6	9.54	79.87	20.130		46,197

2.4 Modules

Both Al-BSF and PERC UMG-Si-based solar cells processed in industrial lines are further assembled into PV modules, following a standard production process, including string formation and tabbing, interconnection, lamination, and finishing. As an example, the average module performance of 72-cell modules is reported in Table 3 with the average values of module production (Forniés et al., 2019).

3 In-field operation of UMG PV modules

PV modules with UMG-Si cells have already been installed in a variety of places around the world. Here, we will report on some controlled tests carried out over large time periods. A demonstration photovoltaic system with UMG-Si modules was installed in Ávila, Spain (Sánchez et al., 2011). The modules were mounted on a fixed structure with an inclination of 45° and south orientation. This PV system consists of three generators of 3.3 kW peak each, two of them with multicrystalline UMG-Si modules of 60 and 72 Al-BSF cells and nominal power ratings of 230 W and 270 W, respectively, and the third one with commercial multicrystalline silicon modules of 60 cells and 230 W which served as a reference. Each of the three generators is connected to a 3.3 kW inverter provided with two maximum power point (MPP) trackers. In this way, the PV system is configured with six strings, each one connected to an MPP tracker.

Figure 14A shows the evolution of the performance ratio (PR) of the system, excluding partial shading intervals, during an operational period of 3 years, with each point representing a 1-

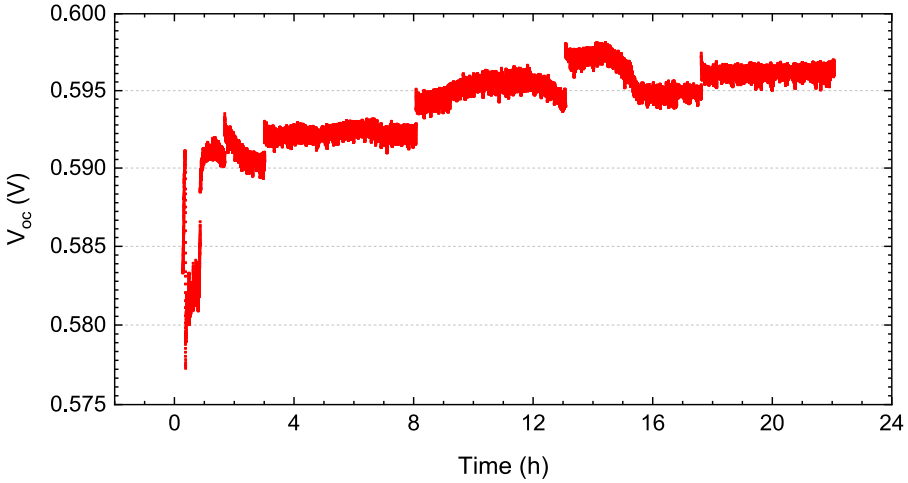

FIGURE 12
V_{OC} evolution of a UMG-Si PERC solar cell under the treatment conditions of injected current and temperature.

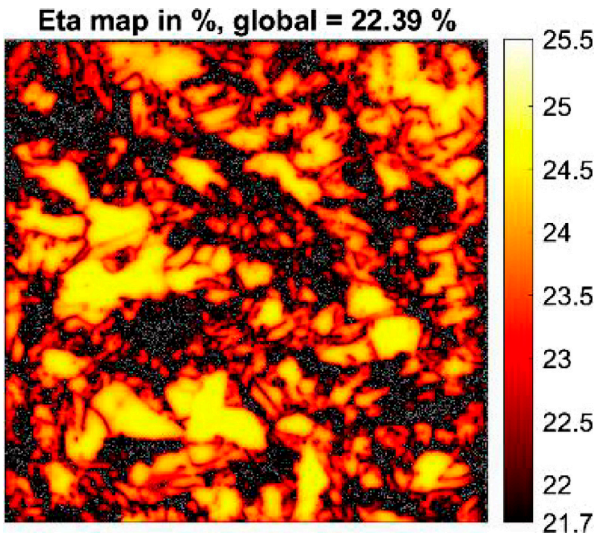

FIGURE 13
Estimated efficiency of UMG-Si solar cells according to the ELBA analysis for a TOPCore structure. The figure was reproduced from the work of Del Cañizo et al. (2023) with permission from the EUPVSEC.

week time lapse. PR values ranged between 0.8 and 0.9 most of the time. The evolution observed is very similar for the three different generators, with a marked seasonal behavior. The PR is lower in summer due to the higher operating temperature of the modules and the lower rainfall. As can be observed, 3 years after the commissioning of the plant, the UMG modules did not show any noticeable degradation over the reference modules based on standard poly-Si.

Another demonstration plant was installed more recently in Tudela (Spain), with seven UMG-Si modules with Al-BSF cells installed in the same rack together with seven commercial modules made of polysilicon-based solar cells (Forniés et al., 2021). Both generators were mounted on a fixed structure with a 30° tilt with respect to the horizontal plane, south-oriented, and completely shadow-free. Each generator was connected to the grid via a 2.5-kW inverter, always operating at MPP. The output power, module temperature, and incoming irradiance were continuously monitored over 24 months of operation so as to calculate the module efficiency and monthly averages of the performance ratio at 25°C (PR25), which are shown in Figure 14B. Results clearly show a very similar behavior of both types of modules (UMG-Si and poly-Si). The inset in Figure 14B shows the annual PR25 average values over 2 years of test. After the first year, the PR25 decreased from 1 to 0.972 for UMG-Si and to 0.976 for poly-Si, which is attributed to the initial LID typical of Al-BSF solar cells (Pingel et al., 2010). After 2 years, the recorded PR25 was even higher for UMG-Si modules (type A, PR25 = 0.980) than for polysilicon modules (PR25 = 0.977).

These results have been further corroborated by Guerra et al. (2022), who calculated the degradation rates of both types of modules over the 2-year period of the study by means of two different procedures, leading to exactly the same result: a mean degradation of around 0.2%/year in the reference poly-Si-based modules (SoG label in the figure), while no measurable degradation was found for UMG-Si modules.

The remarkable conclusion of this work was that no evidence of the existence of any additional degradation mechanism that may eventually affect UMG-Si material could be found.

4 Environmental analysis

To evaluate the differences in the environmental impact associated to the manufacturing of UMG-Si-based cells with respect to other cell technologies based on standard polysilicon, a process-based life-cycle analysis (LCA) has been performed, according to the methodology guidelines on the LCA of photovoltaic electricity published by the International Energy Agency (IEA) and following the Environmental Footprint (EF) 3.0 impact assessment method, as proposed by the European Union (EU) (Official Journal of the European Union, 2013; Fazio et al., 2019; Frischknecht et al., 2020).

TABLE 3 Average values of module production (Forniés et al., 2019).

Cell technology	P_{MAX} [W]	V_{oc} [V]	I_{sc} [A]	V_{MPP} [V]	I_{MPP} [A]	FF (%)	Counts
Al-BSF	325.1	45.73	9.32	37.13	8.76	76.31	1,350
Black Si + PERC	354.4	47.78	9.70	38.21	9.28	77.00	300

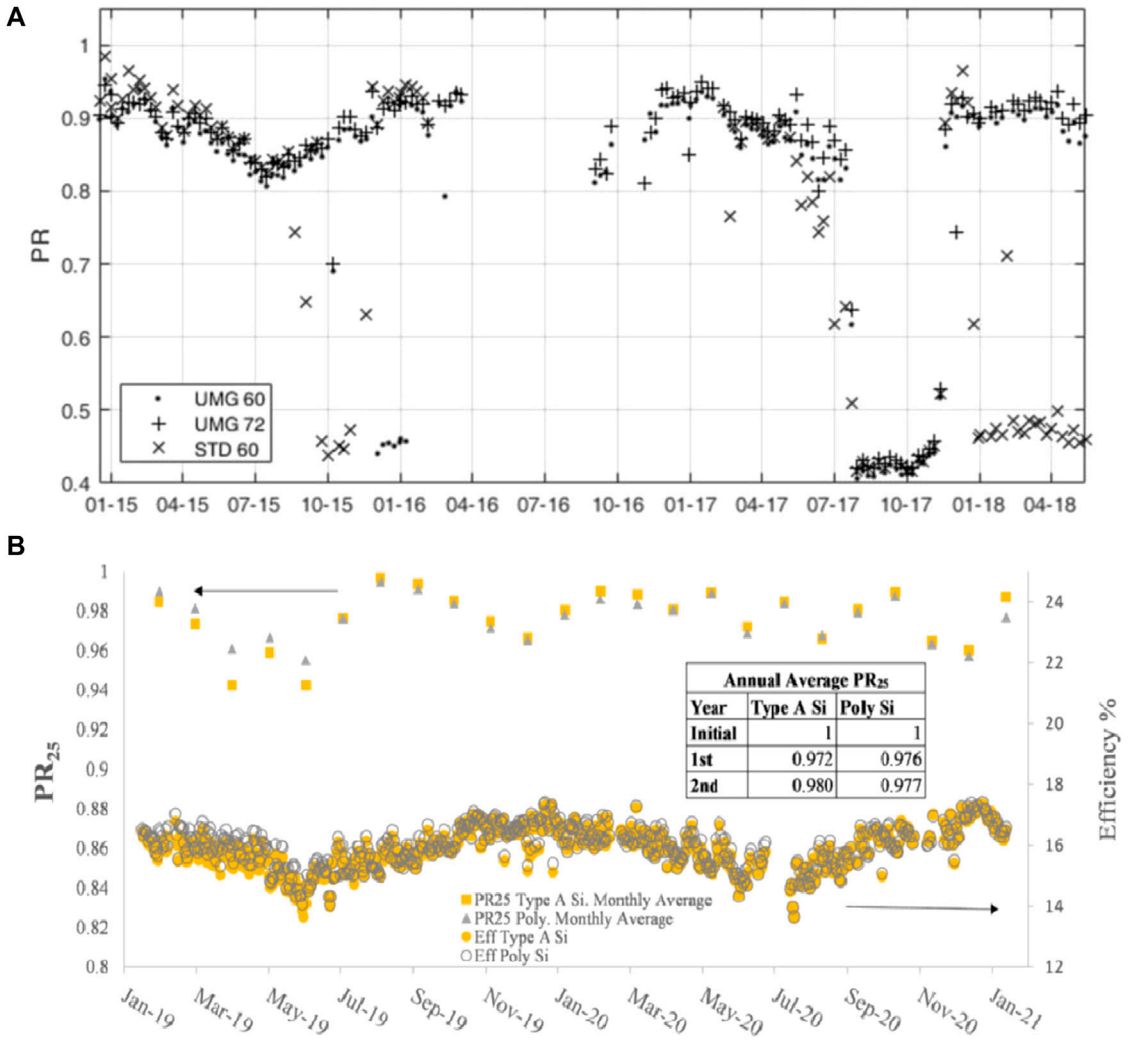

FIGURE 14
(A) Recorded PR of the three generators installed in Avila, Spain, Two of them provided with mc-UMG-Si modules of 60 and 72 cells and the third one with commercial 60 mc-Si cells (STD 60). PR ranges between 0.4 and 0.5 correspond to periods operating with a single string due to issues related to the inverters. The figure was reproduced from the work of Sánchez et al. (2011) with permission. **(B)** Module efficiency and monthly average of PR calculated at 25°C for UMG-Si (type A) and polysilicon recorded over 24 months in operation. Missing data correspond to interventions on the equipment. The figure was reproduced from the work of Forniés et al. (2021) with permission from Elsevier.

It should be noted that this kind of analysis of environmental impact goes beyond the purely scientific and technological relevance, reaching out to other aspects of societal, political, or economic importance. Nevertheless, it turns out that the environmental impact associated with UMG technology is a key aspect justifying its interest, and it is, therefore, relevant to compare UMG Si vs polysilicon in this regard.

In order to proceed with the analysis, it is necessary to refer production to specific energy mixes at relevant production sites, as the electric power input required for manufacturing has a decisive role in the overall impact of the PV value chain (Yue et al., 2014). For this purpose, national electricity mixes have been typically used in the literature, and they will be similarly used here, even though considering them as variables of the study may be controversial and subject to dynamic evolution in the short term. In the following, the reference to specific electricity mixes should not be simply read as representative of the geographical region itself but rather of different constitutional shares of the respective mixes (fossil fuels, renewables,

10.3389/fphot.2024.1331030

TABLE 4 Key parameters for the comparison of the LCA of a PV system with multi-BSF modules, either with UMG or polysilicon substrates.

Module efficiency (%)	Module degradation rate (%)	PV lifetime	BoS lifetime	Annual irradiation	Inclination	Performance ratio (%)	Time frame of data
UMG: 18.43	0.40	30 years	15 years electrical gear	2,160 kWh/m^2/year	Optimal tilt angle 34°	82.50	2015–2020
Poly: 18.55			30 years structure				

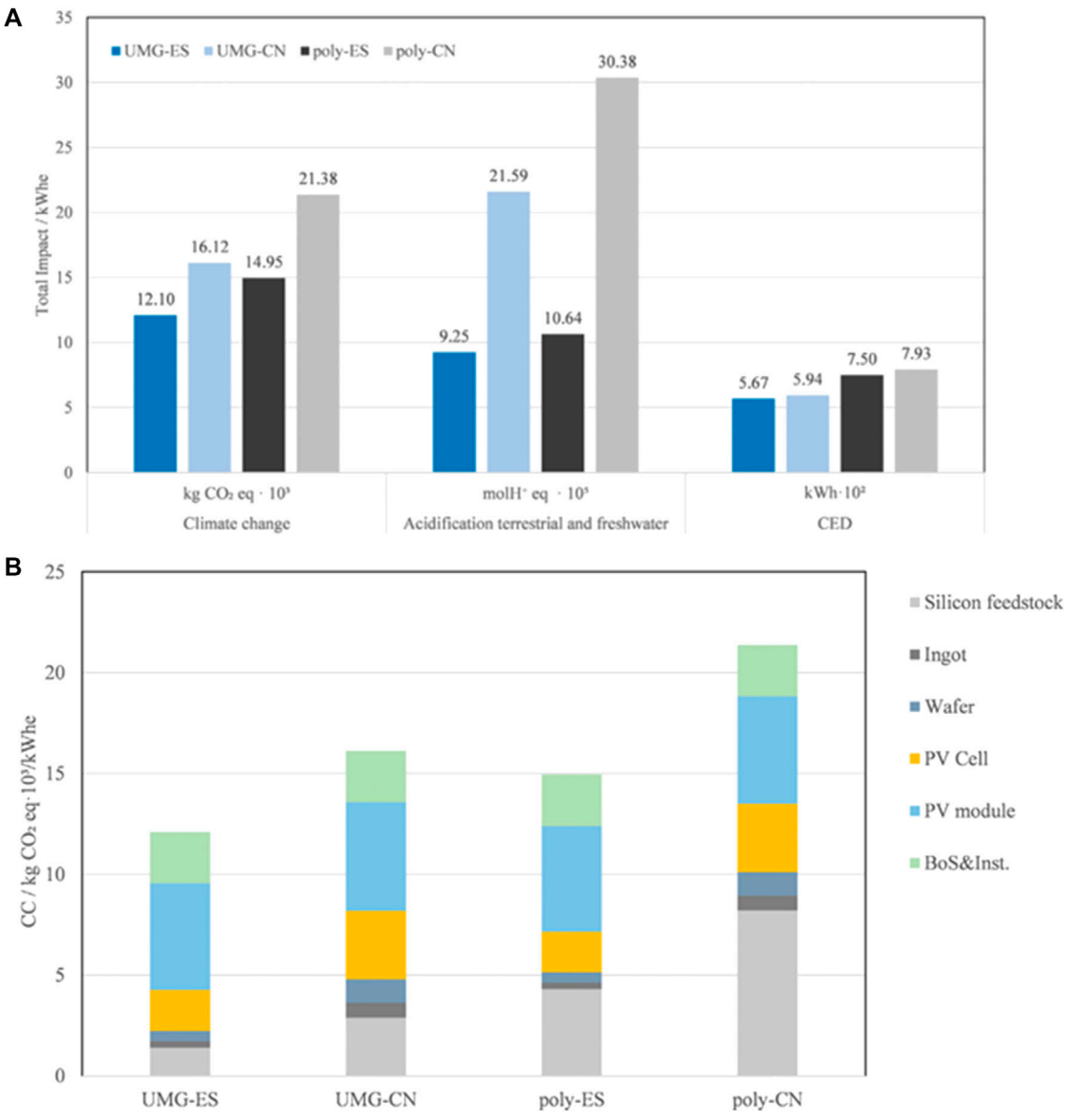

FIGURE 15
(A) The main impacts per kWh of PV-produced electricity for the different scenarios: ES vs CN electricity mix and UMG-Si vs poly-Si material manufacturing. All cases consider Al-BSF cell technology. The figure was reproduced from the work of Méndez et al. (2021) with permission from Elsevier. **(B)** Climate change contributions of different stages of the production of PV systems per kWh of produced electricity, for UMG and polysilicon BSF technologies, when the manufacture is carried out in ES and CN. The figure was reproduced from the work of Méndez et al. (2021) with permission from Elsevier.

TABLE 5 Estimation of the CO_2-payback time of a reference PV system manufactured in CN and ES and located in different European sites.

Location analysis					
Location	Irradiation (kWh/m²/year)	gCO_2eq/kWh		CO_2-payback time (years)	
		Poly-Si CN	UMG-Si ES	Poly-Si CN	UMG-Si ES
Almería (SE Spain)	2,150	21.4	12.1	2.4	1.4
Marseille (SE France)	1,650	27.9	15.8	14.3	8.1
Landes (SW France)	1,350	34	19.3	17.5	9.9
Paris (France)	1,150	40	22.6	20.5	11.6
Lille (France)	1,050	43.8	24.8	22.5	12.7
Frankfurt (Germany)	1,000	46	26	3.1	1.8

TABLE 6 Parameter values used for the evaluated scenarios of the environmental analysis, including different cell architectures.

Work ref. and cell technology	Silicon type	Wafer area (m²)	Cell eff. (%)	Pmax (Wp/cell)	Pmax (Wp/m²)	Module eff. (%)	P_{MAX} (W)	Electricity consumption (kWh/m²)
Forniés et al. (2019), Al-BSF	poly-Si	0.02457	18.50	4.55	185	16.72	324.0	18.31
Forniés et al. (2019), Al-BSF	UMG	0.02489	18.40	4.58	184	16.84	326.4	18.27
Luo et al. (2018), PERC	poly-Si	0.02457	19.20	4.72	191.9	17.34	336.2	24.42
Frischknecht et al. (2020); Frischknecht. (2021), Al-BSF	poly-Si	0.02457	18.80	4.62	188	16.99	329.3	17.7
Del Cañizo et al. (2023), PERC	UMG	0.02457	19.93	4.90	199.3	18.01	349.1	19.13
Del Cañizo et al. (2023), TOPCoRe	UMG	0.02457	22.40	5.50	224	20.24	392.3	20.35

As above, all categories considered in the EF methodology were calculated, with the focus now set on the following categories: CC, ATF, resource use, metals and minerals, and ionizing radiation.

nuclear, *etc.*). Four electricity mixes are used as referent mixes in this section, including dissimilar proportions of primary generation technologies. The Spanish (ES) electricity mix is used as the example of the major proportion of renewable electricity, while the presence of coal is residual. The EU, the US, and China (CN) are used as examples of mixes with increased ratios of non-renewable sources or fossil fuels. European countries are, on average, characterized by around 20% of nuclear energy, which is slightly reduced in the case of the US, while for China's mix, it is almost residual. Likewise, the share of coal generation for the US and EU is around 15%–20%, while it counts for more than 60% of the total generation in China.

The software SimaPro 9.0 is used, with Ecoinvent 3.5 as a database for all the background data (Wernet et al., 2016). Additionally, crystalline silicon solar cell processes are updated, recurring to up-to-date literature when appropriate.

4.1 Environmental analysis of PV systems with UMG-Si Al-BSF modules

For the Al-BSF technology, the LCA covered the whole PV value chain, from metallurgical silicon production to PV-electricity generation, using as a functional unit 1 kWh of electricity produced by a ground-mounted multicrystalline PV system with a nominal capacity of 100 MWp installed in the South of Spain, whose key parameters are summarized in Table 4. The complete study can be consulted in Méndez et al. (2021).

Among the most important results obtained from the study, see Figure 15A, is the verification that the usage of UMG-Si instead of conventional polysilicon can lead to an overall 20% reduction in climate change-related emissions when considering the Spanish (ES) mix (12.10 vs 14.95 $gCO_2eq/kWhe$), which is even higher for the CN mix (16.12 vs 21.38 $gCO_2eq/kWhe$).

Figure 15A complements these results with the impact on acidification: terrestrial and freshwater (ATF) and the calculation of the total cumulative primary energy demand (CED). The energy payback time (EPBT) of the system, which can be deduced from the latter (Louwen et al., 2016), shows similar trends to other impacts, being halved for the case of UMG-Si-based modules manufactured with the Spanish mix as compared to the case of poly-Si-based technology manufactured in China.

Figure 15B shows the corresponding shares of the different manufacturing stages of a full PV system to the climate change emissions for the different scenarios considered. As can be observed, the most significant differences affect the silicon feedstock and the cell fabrication stages, with an important impact on the electricity mix considered. In all cases, UMG-Si outperforms poly-Si for a given mix.

10.3389/fphot.2024.1331030

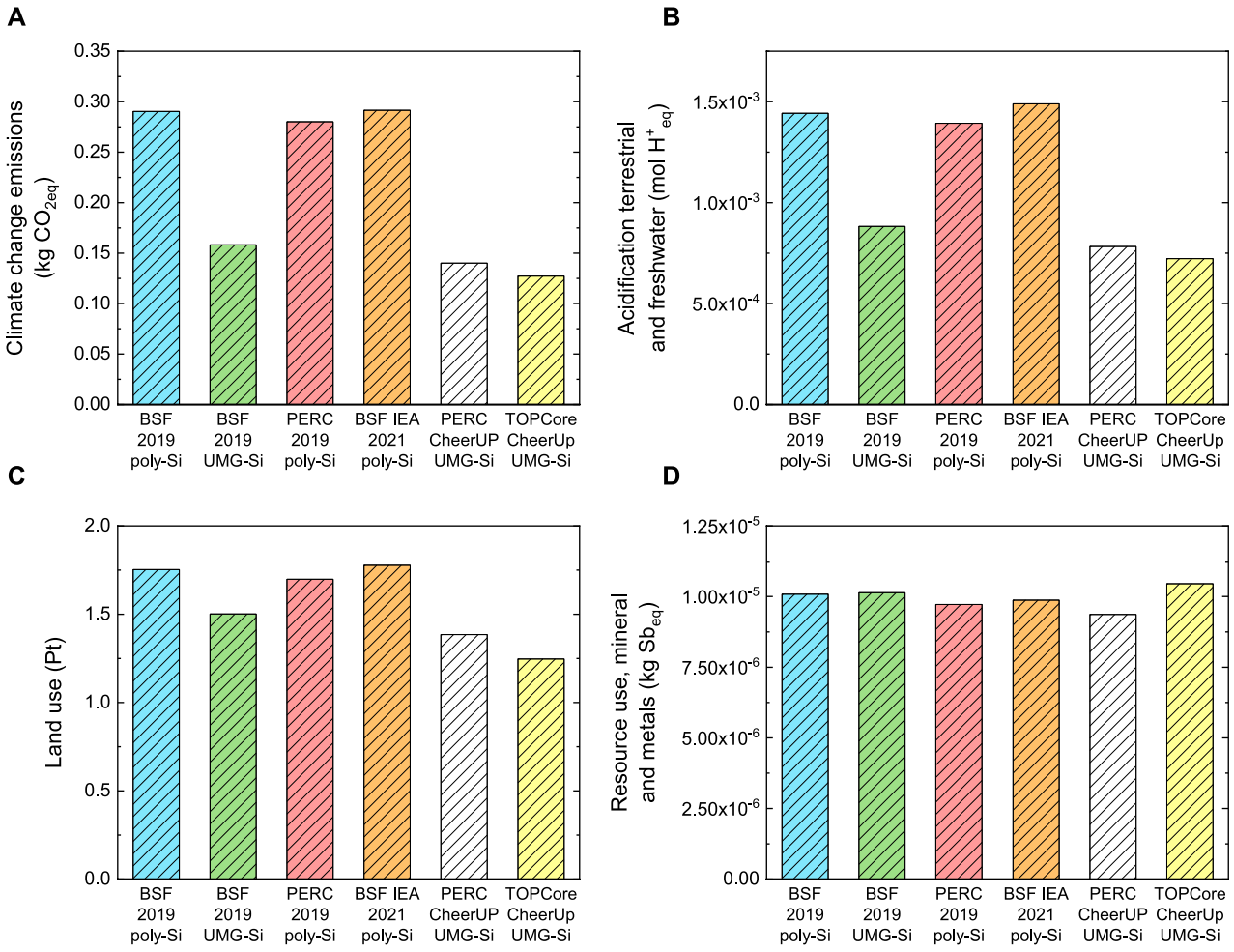

FIGURE 16
Cell processing impacts (in standard units) for the selected categories (ES mix scenario). **(A)** Climate change emissions in kgCO_2eq per cell Wp. **(B)** Acidification terrestrial and freshwater in mol H^+eq per cell Wp. **(C)** Land use in standard units. **(D)** Use of resources in kg Sb eq per cell Wp.

4.2 CO_2-payback time of UMG-Si Al-BSF technology

The composition of the electricity mix at the location of the actual UMG-Si-based PV system is relevant to calculate the CO_2-payback time, *i.e.*, the time required for the system to offset the greenhouse gases emitted as a result of its construction so that it begins saving GHG emissions as compared to the conventional grid-based electricity. The following calculations want to compare this payback time for the UMG-Si- and poly-Si-based systems characterized in the previous section, considering exclusively parameters affecting the PV generator (those module technology- and manufacturing-dependent) and not including others, such as the balance of the system.

The 100-MW photovoltaic generator described in Section 4.1 is used as a reference, locating it in different European places: Almeria (southeast Spain), Marseille (southeast France), Landes (southwest France), Paris (France), Lille (France), and Frankfurt (Germany). These locations have been selected as representative of three different national electricity mixes, with different levels of related emissions: low for France (58 gCO_2eq/kWh), medium for Spain (165 gCO_2eq/kWh), and high for Germany (348 gCO_2eq/kWh), according to data published by the European Environment Agency (www.eea.europa.eu) for 2021. As additional input data, the annual average irradiation (kWh/m^2/year) at the given locations has been considered. The CO_2-payback time results are summarized in Table 5.

The last two columns in the table show the calculated payback time (in years) necessary to counteract the emissions incurred during fabrication of the PV modules. As can be observed, UMG-Si, fabricated in a medium-rate-emission mix like that of Spain, systematically yields lower payback times (~56%) in comparison to poly-Si modules fabricated in China. The time span is obviously largely influenced by the solar resource at the site, but significantly more (approximately 10 times, comparing the cases in France and Germany) by the actual mix to which the PV system is injecting energy.

4.3 Comparison of the environmental impact of different cell technologies

As for the environmental analysis of PERC and TOPCon structures, additional studies have been performed, focused only

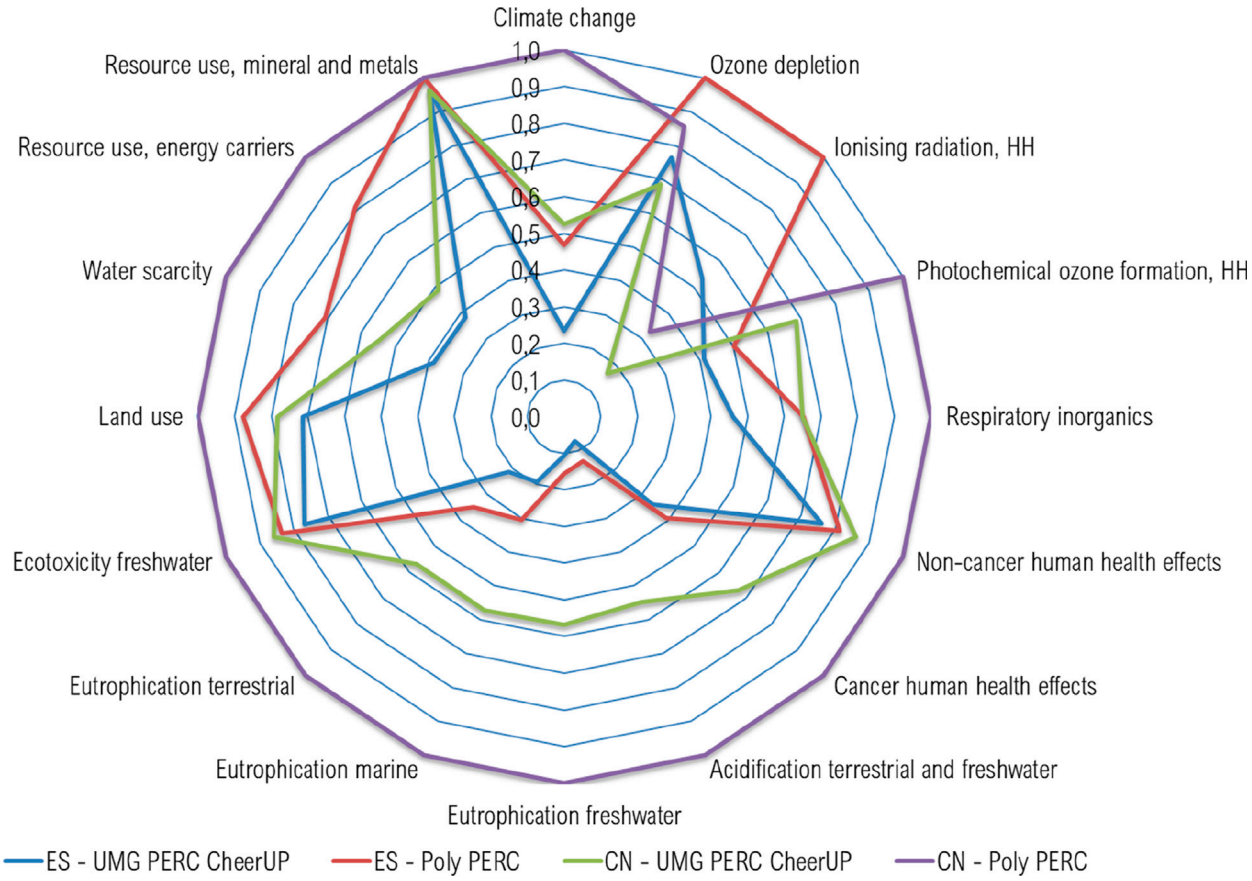

FIGURE 17
Normalized environmental impacts of polysilicon and UMG PERC technologies, comparing the manufacture in ES and CN. The figure was reproduced from the work of Del Cañizo et al. (2023) with permission from the EUPVSEC.

on cell technology and not on full PV systems, in contrast to the previous study. With current cell-to-module factors very close to unity, the conclusions can be safely extrapolated up to the UMG-Si PV module level. Table 6 shows the different schemes of PV cells evaluated, among which both polysilicon and UMG-Si materials are considered. The table includes input data from different sources.

As above, all categories considered in the EF methodology were calculated, with the focus now set on the following categories: climate change (CC), acidification (ATF), resource use, metals and minerals, and ionizing radiation. The results are shown in Figure 16.

Climate change and acidification categories present the most significant differences when comparing silicon feedstocks. UMG-Si shows better performance on both parameters, mainly because its manufacturing process is less energy-intensive, thus leading to lower associated emissions. In the CC category, UMG-Si is in the range of 0.158–0.127 $kgCO_2eq$ per cell, while polysilicon cells generate between 0.292–0.280 $kgCO_2eq$. Within the CC category, the observed improvements are aligned with the progress in cell architectures and their improved efficiencies. However, small differences are found between data sources for BSF cells. The acidification parameter shows a similar trend. Concerning resource use, the results are quite similar, but the TOPCoRe architecture shows a slight increase due to greater necessities related to metallization. In general, TOPCon schemes incur in a larger use of silver and aluminum per peak watt than BSF and PERC.

The trends for the normalized values in all EF categories for PERC architectures considering ES and CH mixes are summarized in Figure 17, revealing the strong influence of the manufacturing location over all the environmental categories considered. The predominant presence of fossil fuels, specifically coal, in the Chinese mix has a strong influence over these results. In the same way, it is concluded that for PERC cells, the use of UMG-Si leads to an approximately 50% reduction in terms of CC emissions for both ES and CN mixes with respect to conventional poly-Si. However, for the ATF category, the reduction is 45% for the ES mix and 76% for the CN mix. Also, it is interesting to notice how, for the CN mix, some categories suffer from sharper changes, such as eutrophication or cancer human health categories. Therefore, the relevance of the silicon feedstock is even more meaningful when the energy mix contains reduced shares of renewable energies.

In order to show in more detail the environmental impact as a function of cell technology, substrate material and electricity mix for some of the most relevant categories, the results are summarized in Figure 18.

For the CC category (Figure 18A), cells made of poly-Si show values between 0.62–0.28 $kgCO_2/Wp$, while for UMG-Si cells, they

10.3389/fphot.2024.1331030

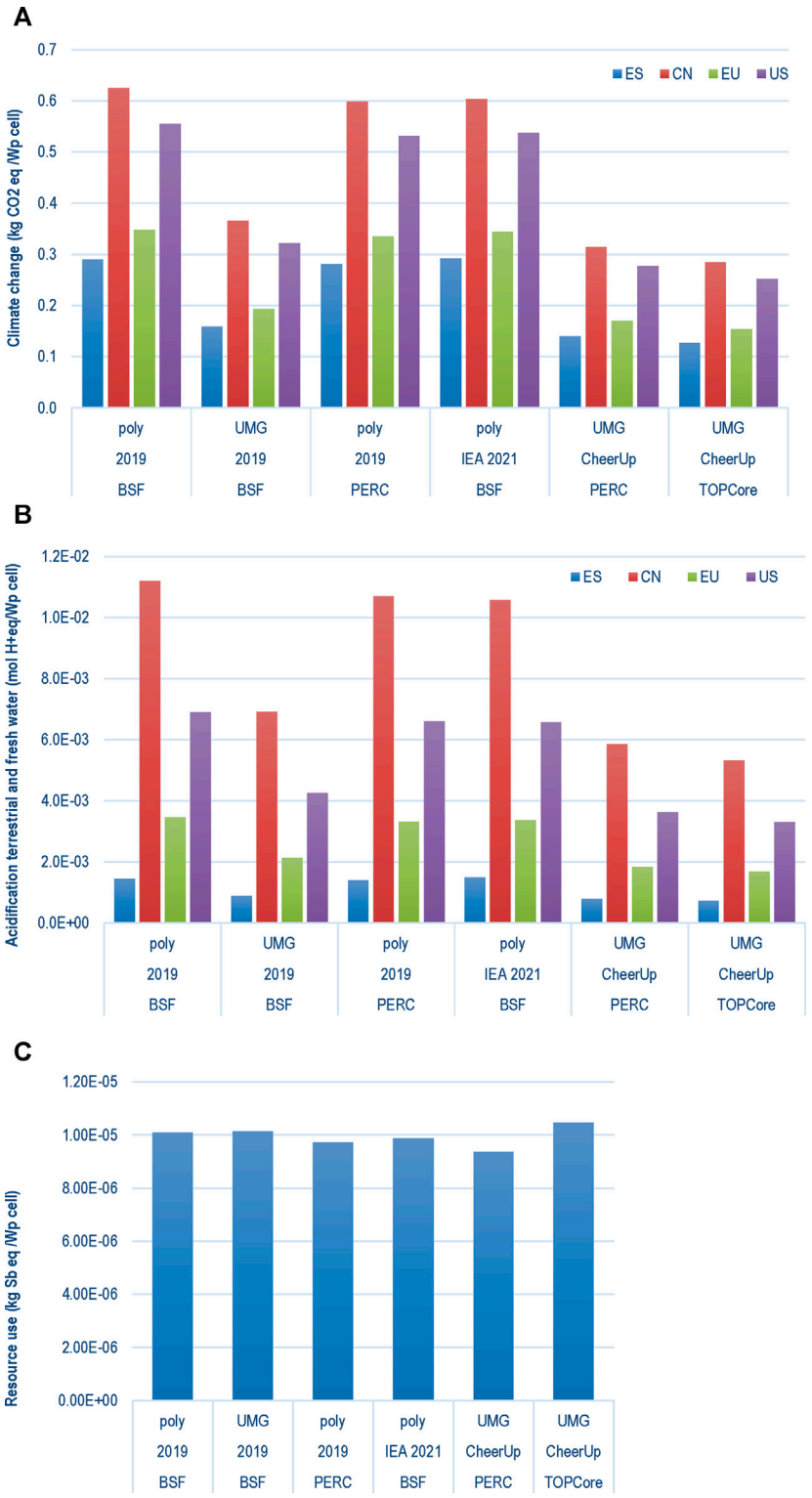

FIGURE 18
Comparison of the environmental impact of conventional polysilicon and UMG-Si technologies for four electricity mixes: ES, CN, EU, and US. **(A)** Climate change emissions in kgCO2eq per cell Wp. **(B)** Acidification terrestrial and freshwater in mol H+eq per cell Wp. **(C)** Use of resources in kg Sb eq per cell Wp.

are 0.37–0.13 $kgCO_2$/Wp. Manufacturing cells in CN, US, and EU mixes imply a 54%, 48%, and 16% increase in climate change emissions, respectively, with respect to the ES mix.

Differences are even more important for the acidification (ATF) category (Figure 18B) on account of the almost negligible proportion of coal in the ES mix. Manufacturing cells in CN, US, and EU mixes

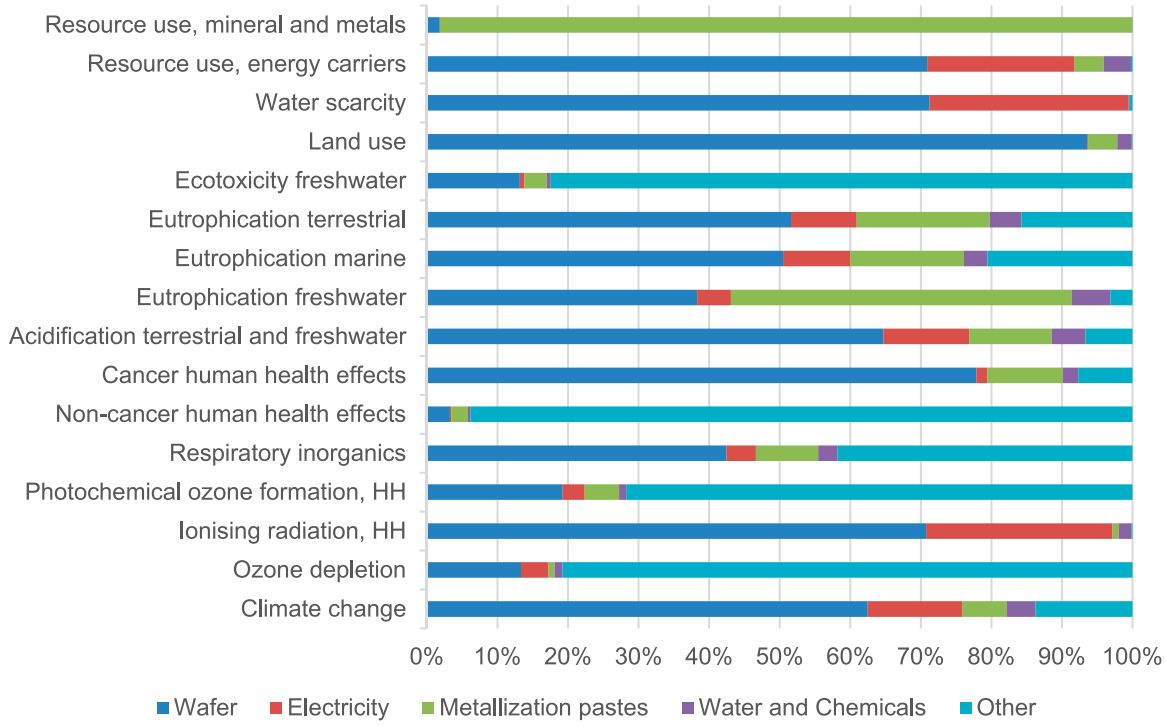

FIGURE 19
Grouped contribution to impact categories (ES—PERC—CheerUp—UMG).

imply 87%, 79%, and 58% higher acidification impact than if fabricated under the ES mix. It must be noticed that both PERC UMG and TOPCoRe-UMG have an ATF impact around 50% lower than poly-BSF for the same electricity mix. In the more uneven case, UMG-PERC cells show 79% and 93% less impact in CC and AFT categories beside poly-BSF (IEA 2021) when ES and CN mixes are selected.

As for resource use of minerals (Figure 18C), the location has not such importance as for CC or AFT since the differences among mixes are less than 0.01%. The use of minerals does not depend on energy mix or location but only on cell technology. Therefore, among UMG cells, PERC and TOPCoRe technologies have a -7.7% and 3.1% rate of resource impact variation as compared to UMG BSF cells, mainly due to the necessity of metallization of each cell architecture and the high levels of optimization achieved for the current PERC cell processing. Contrasting different feedstocks, in this case, UMG PERC and TOPCoRe technologies have a -5.2% and 5.9% rate of resource impact variation when compared to poly-BSF cells. On the other hand, the observed slight differences among BSF cells are probably just due to small parameter variations among different data sources.

As a summary, the grouped environmental impact contributions of UMG-Si PERC cell technology for the Spanish electricity mix scenario are shown in Figure 19.

As can be observed, wafer manufacturing is the most relevant contributor to most environmental impacts, including those related to resource use (energy carriers), water scarcity, acidification, climate change, or ionizing radiation. Electricity consumption, in general, has a lower impact than the wafer, but in some parameters, such as resource use (energy carriers) or ionizing radiation, it becomes more relevant. The electricity use during cell production has no such critical role as compared to wafer production. As could be expected, the main contributions associated with the metallization pastes affect not only the resource use of minerals and metals but also the eutrophication of water. The result is highly influenced by the consumption of metals, specifically silver, in the course of the metallization processes and the eventual contamination that could be produced over freshwater.

5 Conclusion

A proprietary technology for the purification of silicon for solar applications is developed and assessed along the entire value chain, from the feedstock up to the complete PV system.

The purification process involves a number of metallurgical steps (slagging, evaporation, and solidification) to upgrade the purity of metallurgical silicon, resulting in the so-called upgraded metallurgical silicon (UMG-Si). In this material, impurities are present in concentrations compatible with further solar cell processing, the most prominent ones being boron, phosphorus, and metals in concentrations below 0.2 ppmw, 0.3 ppmw, and 0.5 ppmw, respectively. High-performance multicrystalline ingots are produced, showing uniform resistivity along the ingot height due to the addition of gallium, resulting in a compensated material of ~1 Ωcm. Initial bulk lifetimes, in the range of 10 μs, can boost to several hundred microseconds (with a maximum of 722 μs) after an optimized phosphorus diffusion gettering step.

The significant improvement in the UMG-Si electronic quality allowed the achievement of cell efficiencies in the range of those

obtained with conventional polysilicon substrates for industrial-type Al-back surface field (BSF) and passivated emitter and rear cell (PERC) multicrystalline technologies (18.4% and 20.1% as representative efficiency values, respectively). Furthermore, its potential for advanced solar cell technologies beyond PERC is demonstrated, with bulk carrier lifetimes compatible with 22% device efficiency after TOPCore solar cell key thermal steps.

UMG Al-BSF PV modules demonstrated similar performance to reference ones, maintaining PR25 over 0.97 after 2 years of outdoor operation. It is also shown that a conventional regeneration step in manufacturing successfully inhibits light- and elevated temperature-induced degradation for UMG PERC solar cells.

The environmental impact of UMG technology is shown to be lower than that of conventional polysilicon, irrespective of the manufacturing site or the cell technology used, with significant reductions in climate change emissions higher than 20% and simultaneous reductions in the energy payback time of 50%.

In summary, a sustained R&D effort deployed in the last 2 decades has succeeded in demonstrating that UMG-Si can be the basis of a low-CAPEX, low-cost, environment-friendly supply of PV silicon.

Author contributions

JM: writing–review and editing, data curation, investigation, methodology, and validation. VH: writing–review and editing, data curation, investigation, methodology, and validation. EF: writing–original draft, writing–review and editing, data curation, investigation, methodology, and validation. LM: validation, writing–original draft, writing–review and editing, data curation, investigation, and methodology. MT: writing–review and editing, data curation, investigation, methodology, and validation. FR: writing–review and editing, data curation, investigation, methodology, and validation. MF: writing–review and editing, data curation, investigation, methodology, and validation. CD: writing–original draft, writing–review and editing, conceptualization, data curation, formal analysis, funding acquisition, investigation, methodology, project administration, resources, and supervision. DF: writing–original draft, writing–review and editing, conceptualization, data curation, formal analysis, funding acquisition, investigation, methodology, project administration, resources, and supervision. ND: writing–original draft, writing–review and editing, conceptualization, data curation, formal analysis, investigation, and methodology. LC: writing–review and editing, investigation, and methodology. BA: writing–review and editing, data curation, funding acquisition, investigation, methodology, software, and validation. RT: writing–review and editing, data curation, investigation, methodology, supervision, and validation. HC: writing–review and editing, data curation, investigation, methodology, and validation. GS: writing–review and editing, data curation, investigation, methodology, software, supervision, and validation.

Funding

The authors declare that financial support was received for the research, authorship, and/or publication of this article. This work was partially funded as part of the R&D SOLAR-ERA.NET Cofund 2 project CHEER-UP, funded by the Spanish MCIN/AEI/10.13039/501100011033/through projects PCI 2019-111834-2 and PCI 2019-111903-2, by the Spanish Centro para el Desarrollo Tecnológico Industrial (CDTI), and by the Turkish TÜBITAK through Project 219M029. MCIN/AEI/10.13039/501100011033 is also acknowledged for financial support through the GREASE project (PID2020-113533RB-C31).

Conflict of interest

Authors JM and VH were employed by the company FerroGlobe. Authors LM, MT, FR, and MF were employed by the company Aurinka Photovoltaic Group.

The remaining authors declare that the research was conducted in the absence of any commercial or financial relationships that could be construed as a potential conflict of interest.

Publisher's note

References

Aulich, H. A., and Schulze, F. (2002). Crystalline silicon feedstock for solar cells. *Prog. Photovoltaics Res. Appl.* 10 (2), 141–147. Available at:. doi:10.1002/pip.415

Ballif, C., Huijic, D. M., Hessler-Wyser, A., and Willeke, G. (2002). "Nature of the Ag-Si interface in screen-printed contacts: a detailed transmission electron microscopy study of cross-sectional structures," in Conference Record of the Twenty-Ninth IEEE Photovoltaic Specialists Conference 2002, New Orleans, LA, USA, May, 2002 (IEEE), 360–363. Available at:. doi:10.1109/PVSC.2002.1190533

Catalán-Gómez, S., Dasilva-Villanueva, N., Fuertes Marrón, D., and del Cañizo, C. (2021). Phosphorous diffusion gettering of trapping centers in upgraded metallurgical-grade solar silicon. *Phys. status solidi (RRL) – Rapid Res. Lett.* 15, 2100054. doi:10.1002/pssr.202100054

Ceccaroli, B., Øvrelid, E., and Pizzini, S. (2017). *Solar silicon processes: technologies, challenges, and opportunities*. Boca Raton, Florida, United States: CRC Press.

Cocco, F., Grosset-Bourbange, D., Rivat, P., Quost, G., Degoulange, J., Einhaus, R., et al. (2013). "PhotoSil UMG silicon: industrial evaluation by multi-c p-type ingots and solar cells," in 28th European Photovoltaic Solar Energy Conference and Exhibition Proceedings, Paris, France, September, 2002, 4. Available at:. doi:10.4229/28thEUPVSEC2013-2BV.3.21

Dasilva-Villanueva, N., Catalán-Gómez, S., Fuertes Marrón, D., Torres, J. J., García-Corpas, M., and del Cañizo, C. (2022). Reduction of trapping and recombination in upgraded metallurgical grade silicon: impact of phosphorous diffusion gettering. *Sol. Energy Mater. Sol. Cells* 234, 111410. doi:10.1016/j.solmat.2021.111410

Del Cañizo, C., Fuertes Marrón, D., Dasilva-Villanueva, N., Caballero, L. J., Arıkan, B., Canar, H. H., et al. (2023). "Development of low-cost high-efficient and reliable UMG PV cells," in 40th European Photovoltaic Solar Energy Conference, Lisbon, Portugal, September, 2023.

Del Cañizo, C., Luque, A., Bullón, J., Miranda, Á., Míguez, J. M., Riemann, H., et al. (2005) 'Integral procedure for the fabrication of solar cells on solar silicon', in.

20th European Photovoltaic Solar Energy Conference, Barcelona, Spain. June, 2005,

Dietl, J. (1987). "Metallurgical ways of silicon meltstock processing," in *Materials processing: theory and practices* (Amsterdam, Netherlands: Elsevier), 285–352. Available at:. doi:10.1016/B978-0-444-87024-7.50013-5

Fazio, S., Biganzoli, F., Laurentiis, V. de, Zampori, L., Sala, S., and Diaconu, E. (2019). Supporting information to the characterisation factors of recommended EF Life Cycle Impact Assessment methods. Available at: https://publications.jrc.ec.europa.eu/repository/handle/JRC114822.

Forniés, E., Ceccaroli, B., Méndez, L., Souto, A., Pérez Vázquez, A., Vlasenko, T., et al. (2019). Mass production test of solar cells and modules made of 100% UMG silicon. 20.76% record efficiency. *Energies* 12 (8), 1495. Available at:. doi:10.3390/en12081495

Forniés, E., del Cañizo, C., Méndez, L., Souto, A., Pérez Vázquez, A., and Garrain, D. (2021). UMG silicon for solar PV: from defects detection to PV module degradation. *Sol. Energy* 220, 354–362. Available at:. doi:10.1016/j.solener.2021.03.076

Forniés, E., Souto, A., Vlasenko, T., Vázquez, A. P., Tojeiro, M., Anoshenko, M., et al. (2018). "Performance of modules and solar cells made of 100% solar silicon purified by direct route," in Proceedings of the 35th European PV Solar Energy Conference and Exhibition, Munchen, Germany, September, 2018, 24–28. Available at:. doi:10.4229/35thEUPVSEC20182018-2AV.1.5

Frischknecht, R. (2021). Environmental life cycle assessment of electricity from PV systems. Fact sheet. IEA-PVPS. Available at: https://iea-pvps.org/fact-sheets/factsheet-environmental-life-cycle-assessment-of-electricity-from-pv-systems/.

Frischknecht, R., Stolz, P., Heath, G., Raugei, M., Sinha, P., and De Wild-Scholten, M. (2020). *Methodology Guidelines on life cycle assessment of photovoltaic*. Paris, France: IEA. Available at:. doi:10.13140/RG.2.2.15574.88648

Guerra, M. R., De La Parra Laita, I., Solano, M. G., and Pascual, J. (2022). In-field energy performance of solar PV module made of UMG silicon. *IEEE J. Photovoltaics* 12 (5), 1109–1115. doi:10.1109/JPHOTOV.2022.3181499

Hoffmann, V., Míguez Novoa, J. M., Bullón, J., and Buchovska, I. (2015). "Effect of total dopant concentracion on the efficiency of solar cells made of CS Silicon™," in 31st European Photovoltaic Solar Energy Conference, Hamburg, Germany, September, 2015.

Hoffmann, V., Petter, K., Djordjevic-Reiss, J., Enebakk, E., Håkedal, J. T., Tronstad, R., et al. (2008). "First results on industrialization of elkem solar silicon at pillar JSC and Q-cells," in 23rd EU PVSEC, Valencia, Spain, September, 2008.

IEC (2022). IEC TS 63342 — C-Si photovoltaic (PV) modules — light and elevated temperature induced degradation (LETID) test — detection. Available at: https://webstore.iec.ch/publication/67332.

Louwen, A., Van Sark, W. G. J. H. M., Faaij, A. P. C., and Schropp, R. E. I. (2016). Re-assessment of net energy production and greenhouse gas emissions avoidance after 40 years of photovoltaics development. *Nat. Commun.* 7 (1), 13728. doi:10.1038/ncomms13728

Luo, W., Khoo, Y. S., Hacke, P., Naumann, V., Lausch, D., Harvey, S. P., et al. (2017). Potential-induced degradation in photovoltaic modules: a critical review. *Energy & Environ. Sci.* 10 (1), 43–68. Available at:. doi:10.1039/C6EE02271E

Luo, W., Khoo, Y. S., Kumar, A., Low, J. S. C., Li, Y., Tan, Y. S., et al. (2018). A comparative life-cycle assessment of photovoltaic electricity generation in Singapore by multicrystalline silicon technologies. *Sol. Energy Mater. Sol. Cells* 174, 157–162. Available at:. doi:10.1016/j.solmat.2017.08.040

Méndez, L., Forniés, E., Garrain, D., Pérez Vázquez, A., Souto, A., and Vlasenko, T. (2021). Upgraded metallurgical grade silicon and polysilicon for solar electricity production: a comparative life cycle assessment. *Sci. Total Environ.* 789, 147969. doi:10.1016/j.scitotenv.2021.147969

Michl, B., Rüdiger, M., Giesecke, J. A., Hermle, M., Warta, W., and Schubert, M. C. (2012). Efficiency limiting bulk recombination in multicrystalline silicon solar cells. *Sol. Energy Mater. Sol. Cells* 98, 441–447. Available at:. doi:10.1016/j.solmat.2011.11.047

Modanese, C., Di Sabatino, M., Søiland, A.-K., Peter, K., and Arnberg, L. (2011). Investigation of bulk and solar cell properties of ingots cast from compensated solar grade silicon. *Prog. Photovoltaics Res. Appl.* 19 (1), 45–53. Available at:. doi:10.1002/pip.986

Official Journal of the European Union, (2013). Commission Recommendation of 9 April 2013 on the use of common methods to measure and communicate the life cycle environmental performance of products and organisations. Available at: https://eur-lex.europa.eu/legal-content/EN/TXT/PDF/?uri=CELEX:32013H0179&from=EN.

Øvrelid, E., Geerligs, B., Jensen, R., Tang, K., Santeen, S., and Wiersma, B. (2006). Solar grade silicon by a direct metallurgical process. *Silicon Chem. industry VIII*, 223–235.

Pingel, S., Koshnicharov, D., Frank, O., Geipel, T., Zemen, Y., Striner, B., et al. (2010). "Initial degradation of industrial silicon solar cells in solar panels," in 25th European Photovoltaic Solar Energy Conference, Valencia, Spain, September, 2010.

Richter, A., Müller, R., Benick, J., Feldmann, F., Steinhauser, B., Reichel, C., et al. (2021). Design rules for high-efficiency both-sides-contacted silicon solar cells with balanced charge carrier transport and recombination losses. *Nat. Energy* 6 (4), 429–438. Available at:. doi:10.1038/s41560-021-00805-w

Sánchez, E., Torreblanca, J., Carballo, T., Parra, V., Bullón, J., Míguez, J. M., et al. (2011). Outdoor monitoring of the energy yield and electrical parameters of standard polysilicon based and new umg-Si PV modules. *Energy Procedia* 8, 503–508. doi:10.1016/j.egypro.2011.06.173

Wernet, G., Bauer, C., Steubing, B., Reinhard, J., Moreno-Ruiz, E., and Weidema, B. (2016). The ecoinvent database version 3 (part I): overview and methodology. *Int. J. Life Cycle Assess.* 21 (9), 1218–1230. Available at:. doi:10.1007/s11367-016-1087-8

Yue, D., You, F., and Darling, S. B. (2014). Domestic and overseas manufacturing scenarios of silicon-based photovoltaics: life cycle energy and environmental comparative analysis. *Sol. Energy* 105, 669–678. doi:10.1016/j.solener.2014.04.008

Yuge, N., Abe, M., Hanazawa, K., Baba, H., Nakamura, N., Kato, Y., et al. (2001). Purification of metallurgical-grade silicon up to solar grade. *Prog. Photovoltaics Res. Appl.* 9 (3), 203–209. Available at:. doi:10.1002/pip.372